IEEE Access
Multidisciplinary | Rapid Review | Open Access Journal

Received September 15, 2018, accepted September 29, 2018, date of publication October 8, 2018,
date of current version November 19, 2018.

Digital Object Identifier 10.1109/ACCESS.2018.2873713

Adaptive Weighted Total Variation Minimization Based Alternating Direction Method of Multipliers for Limited Angle CT Reconstruction

FULIN LUO[1,2], (Member, IEEE), WEICHEN LI[1], WEIPING TU[1], AND WEIWEN WU[3]

[1]School of Computer Science, Wuhan University, Wuhan 430072, China
[2]State Key Laboratory of Information Engineering in Surveying, Mapping and Remote Sensing, Wuhan University, Wuhan 430079, China
[3]Key Laboratory for Optoelectronic Technology and Systems, Ministry of Education, Chongqing University, Chongqing 400044, China

Corresponding author: Weiping Tu (tuweiping@whu.edu.cn)

This work was supported in part by the National Science Foundation of China under Grant 61801336, in part by the National Postdoctoral Program for Innovative Talents under Grant BX201700182, and in part by the China Postdoctoral Science Foundation under Grant 2017M622521.

ABSTRACT In CT image reconstruction, the limited angle problem is an ill-posed problem. To solve this ill-posed problem, the total variation (TV) regularization has been widely used in image reconstruction. In recent years, an algorithm based on TV regularization and alternating direction multiplier method has been proposed and named as ADTVM. ADTVM can reconstruct high-quality images for the limited angle problem. However, ADTVM just considers the homogeneity of image at different directions. In real application, image possesses different properties at different directions. Therefore, we construct an adaptive weighted TV (AwTV) regularization and propose the ADM-AwTV method on the basis of ADTVM. ADM-AwTV is an iterative image reconstruction method which can reveal the anisotropy of image, adaptively. In each iteration, the weights of different directions can update according to the last reconstruction image. Experiments on two simulation images and one real projection data show that the proposed method achieves better reconstruction results than the other iterative image reconstruction methods such as ART-TV and ADTVM for the limited angle problem.

INDEX TERMS CT image reconstruction, limited angle, alternating direction method of multipliers, adaptive weighted total variation.

I. INTRODUCTION

Computed tomography (CT) is a technique that uses a special device to collect projection data from an object, and then a reconstruction algorithms is used to obtain a tomographic image of the object [1]–[3]. The CT image, which is used to detect the internal structure of target object without damage [4], [5], is differ from the nature image, the multispectral image and the hyperspectral image that just can obtain the surface information of target object [6]–[10]. For the image reconstruction algorithms, they can be divided into two categories including analytical reconstruction and iterative reconstruction [11]. The analytic algorithm needs the completeness of the projection data that must be enough collected by the CT devices [12], [13]. The filtered back projection (FBP) algorithm is a classic analytic method that can quickly and accurately reconstruct the image with the sufficient projection data [14]–[16]. However, in real application, the CT devices are often affected by various factors such as device characteristics, X-ray dose, special requirements, etc., which cannot collect complete projection data, that is to say, they can only obtain the projection data at incomplete angles. The analytic algorithms with incomplete angles often result in the artifacts with different shapes, which seriously affect the quality of reconstructed image [17], [18]. Therefore, the iterative algorithms were proposed to reconstruct image with the incomplete projection data in 1970s [19]–[21]. These algorithms can be used to eliminate the artifacts with different iterative steps, such as ART (algebraic reconstruction technique) [22] and MLEM (maximum likelihood expectation maximization) [23], [24]. However, these methods cost much running time for the large number of iterations.

In recent years, the compressive sensing (CS) theory has been widely used in signal or image reconstruction [25]–[30]. For the signal reconstruction, we can use a few information to well recover the signal, and some classic methods includes orthogonal matching pursuit (OMP) [31], orthogonal least squares (OLS) [32], and l_p-minimization problem [33]. For the image reconstruction, the discrete image with a small amount of sampling can be accurately recovered with a CS algorithm, such as prior image constrained CS (PICCS) and its improved methods [34]–[36]. The total variation (TV) minimization is a regularization method that uses the idea of CS theory [37]–[39]. TV is often used to optimize various image reconstruction algorithms in recent years [40]–[43]. Shahid *et al.* [44] and Wang *et al* [45] proposed some total variation methods based on the graph structures, and these methods achieved satisfactory results for tomographic reconstruction. Wang *et al.* [46] designed a reweighted anisotropic TV to better solve the limited-angle CT image reconstruction. Chen *et al.* [47] generated a dynamic PET image reconstruction method based on the low-rank and sparse matrix decomposition. Du *et al.* [48], Wang [49], and Wang *et al.* [50] proposed a sparse optimization algorithm that combines the total variation minimization and the alternating direction method, termed ADTVM. With the idea of alternating direction [51]–[54], ADTVM divides the image reconstruction problem into several sub-problems. Firstly, the TV model [55]–[57] is transformed into an equivalent optimization problem with constraint through variable substitution. Then, the augmented Lagrange multiplier method is used to decompose the original problem into two sub-problems for obtaining analytic solution. Finally, the alternating direction method is used to minimize the augmented Lagrangian function and obtain a reconstruction image. ADTVM can obtain better image for the limited angle problem. However, the algorithm considers that the image possesses the same property in different directions, which cannot effectiveness representation the differences of different direction.

In recent years, many reconstruction algorithms based on new TV regularization have been proposed [46], [58], [59]. To reveal the anisotropy of image, we improved the TV regularization in ADTVM and proposed an adaptive weighted TV algorithm based on ADMTV, called ADM-AwTV. This method possesses different weights in different directions, and the weights are adaptively obtained from each iterative image to represent different properties of image in different directions. With the improvement of TV model, some experiments for multiple image reconstruction demonstrate that the proposed algorithm can obtain better reconstructed accuracy and faster convergence speed in limited angles compared with two related methods.

The remainder of the paper is organized as follows: In Section II, we summarize some related theories including compressed sensing, TV regularization, ADMM. Then, the proposed ADM-AwTV method is descripted in Section III. In Section IV, some experiments are conducted on two phantom images and one real projection data, and some classical algorithms is used to demonstrate the effectiveness of the proposed method for the limited angle problem. Finally, in Section V, we draw the conclusions of this paper as well as an outlook for the future work.

II. RELATED WORKS

In this section, we first introduces the basic theoretical knowledge about CS used in CT image reconstruction. Then, we introduces the TV regularization and alternating direction method of multipliers (ADMM) to generate the ADTVM method.

A. COMPRESSIVE SENSING (CS)

In 2006, Donoho [60] proposed the theory of compressed sensing. The theory considers that a signal can be recovered by a small number of samples that are very sparse in high probability and accurately with a series of operations. In medical CT, the compressed sensing technique can shorten the acquisition time of projection data, so that the patients are just exposed to X-rays in a shorter time. Therefore, with the CS reconstruction methods, the diagnosis process is safer and more reasonable, and the data storage space and the transmission time will be reduced.

According to CS, the image reconstruction method can be defined as the following minimum problem a constraint.

$$\begin{aligned} &\min_{f} |\Psi f|_{l_1} \\ &\text{s.t. } p = Wf \end{aligned} \tag{1}$$

where Ψ is the sparse transform and f is the vector of the target image. The matrix W is a system matrix describing the X-ray projection measurements. p is the line integral value sampled by the device—the projected sinogram vector in CT. Since CS image reconstruction is to reconstruct the sparse image possessing the minimized l_1 norm, it is necessary to find a sparse transform to sparsely represent the information of an image. There are three types of sparse transform methods including DCT (discrete cosine transform), DWT (discrete wavelet transform), and DGT (discrete gradient transform).

In CT image reconstruction, the image approximately tends to the characteristics of continuous slices, in which the gradient of the image is sparse, so that we can use the DGT to represent the reconstructed image, and the minimized total variation of the image is used to restore the image with high probability and accuracy.

B. TOTAL VARIATION (TV) REGULARIZATION

Regularization is essentially to address an ill-posed objective function, which adds a regular term after this function to make the ill-posed problem become well-posedness. Image reconstruction is an inverse problem, while the image reconstruction based finite angle is an ill-posed problem. Therefore, the finite reconstruction problem can be effectively solved by using regularization.

The linear equations for image reconstruction can be represented as the following.

$$Wf = p \tag{2}$$

Generally, the solution can be obtained by $\|Wf - p\|_2$. However, this problem for the finite angle is ill-posed. Therefore, a penalty is added after the objective function to obtain a well-posed objective function, and the function can be denoted as the following.

$$C_\Omega = \|Wf - p\|_2^2 + \alpha\Omega(f) \tag{3}$$

where $\alpha > 0$ is the regularization parameter. $\Omega(f)$ is the regularization function and can be defined as TV.

$$\Omega(f) = \|f\|_{TV} = \int_{\pi_f} |\nabla_f| \, dxdy = \int_{\pi_f} \sqrt{f_x^2 + f_y^2} dxdy \tag{4}$$

where TV is the integral of the gradient value of image. π_f is the range of image. f_x and f_y are the partial derivative of image.

C. ADMM

ADMM was proposed in the 1970s, and it was originally used to solve partial differential equations. In 2011, Boyd *et al.* [61] demonstrate that ADMM is suitable for the optimization of large-scale distributed problems. It has been widely used in machine learning for the convex optimization problems with constraints. ADMM can divide a large problem, which is difficult to obtain the optimized solution, into several sub-problems. Then the solution of the original problem can be obtained by solving these sub-problems, alternately.

ADMM is an augmented Lagrangian multiplier method. Therefore, an augmented Lagrangian function can be constructed, and the alternating direction is used to solve the function. For example, a convex optimization problem can be expressed as:

$$\min_{x,y} f(x) + g(y), s.t. Ax + By = b \tag{5}$$

The Lagrangian function for this problem is:

$$L(x, y, \lambda) = f(x) + g(y) - \lambda^T(Ax + By - b) + \frac{c}{2}\|Ax + By - b\|_2^2 \tag{6}$$

To solve this problem without the alternating direction method, the Lagrangian function can be solved as follows:

$$\begin{cases} (x^{k+1}, y^{k+1}) = \arg\min_{x,y} L(x, y; \lambda^k) \\ \lambda^{k+1} = \lambda^k - c(Ax^{k+1} + By^{k+1} - b) \end{cases} \tag{7}$$

After using the alternating direction method, the optimized problem can be divided into the following sub-problems:

$$\begin{cases} x^{k+1} = \arg\min_{x} L(x, y; \lambda^k) \\ y^{k+1} = \arg\min_{y} L(x, y; \lambda^k) \\ \lambda^{k+1} = \lambda^k - c(Ax^{k+1} + By^{k+1} - b) \end{cases} \tag{8}$$

D. ADTVM

According to the TV regularization, the optimization function can be denoted as the following with a constraint.

$$\begin{aligned} &\arg\min \Omega(f) = \min \|f\|_{TV} \\ &\text{s.t. } \|Wf - p\| \le \varepsilon \end{aligned} \tag{9}$$

where ε is a constant indicating the error between the computational projection data and the real projection data.

For the TV optimization problem, it is very difficult to find the optimization solution. To address this problem, the TV model can be transformed as a sparse optimization problem with two difference operators. The alternating direction method can be used to solve the sparse optimization algorithm and the ADMTV method can be constructed. Therefore, the TV optimization problem can be represented as:

$$\begin{aligned} &\arg\min \|f\|_{TV} = \min \sum_i \|D_i f\|_1 \\ &\text{s.t. } \|Wf - p\| \le \varepsilon \end{aligned} \tag{10}$$

where D_i is the difference operator matrix in a direction.

Let $u_i = D_i f$, and the sparse optimization problem can be denoted as:

$$\begin{aligned} &\arg\min \sum_i \|u_i\|_1 \\ &\text{s.t. } \|Wf - p\| \le \varepsilon, u_i = D_i f \end{aligned} \tag{11}$$

The Lagrangian function of the sparse optimization can be constructed as follows:

$$\begin{aligned} &L(f, u_i, v_i, \lambda) \\ &= \sum_i \left(\|u_i\| - v_i^T (D_i f - u_i) + \frac{\beta_i}{2} \cdot \|D_i f - u_i\|_2^2 \right) \\ &\quad - \lambda^T (Wf - p) + \frac{\mu}{2} \cdot \|Wf - p\|_2^2 \end{aligned} \tag{12}$$

where β_i and μ are the parameters to control the weight, and v_i and λ are two Lagrangian multipliers vectors.

According to ADMM, the Lagrangian function can be divided into "u-subproblem" and "f-subproblem" by separating the variables u_i and f.

$$\begin{aligned} &\min_{u_i} L(u_i) \\ &= \sum_i \left(\|u_i\|_1 - v_i^T (D_i f - u_i) + \frac{\beta_i}{2} \cdot \|D_i f - u_i\|_2^2 \right) \end{aligned} \tag{13}$$

$$\begin{aligned} &\min_{f} L(f) \\ &= \sum_i \left(-v_i^T (D_i f - u_i) + \frac{\beta_i}{2} \cdot \|D_i f - u_i\|_2^2 \right) \\ &\quad - \lambda^T (Wf - p) + \frac{\mu}{2} \cdot \|Wf - p\|_2^2 \end{aligned} \tag{14}$$

The "u-subproblem" can be solved using the iterative soft thresholding function. The "f-subproblem" sets the partial derivative of f to zero. Then, the optimization solution can be obtained by updating u_i, f and two Lagrangian multipliers v_i and λ, alternately.

III. METHODOLOGY

For the ill-posed problem in CT image reconstruction, the classical method is to add a regularization term. The ADTVM algorithm combines the TV regularization and the ADMM method, which has a good effect for the limited angle problem. This method just considers the image has the same property in different directions. However, in real image, it generally possesses different properties in different directions. Therefore, we can set different weights in different directions to reveal the anisotropy of image. To adaptively represent the anisotropy, we propose the ADM-AwTV method by obtaining the weights of different directions, adaptively.

A. AWTV REGULARIZATION

According to the TV regularization, the difference operators of the TV model has the same value, which indicates that this TV model possesses the isotropy for the reconstructed image. To represent the anisotropy of image, we propose an adaptive weighted TV for image reconstruction, and the AwTV can be defined as the following.

$$\begin{aligned}\Psi(f) &= \|f\|_{AwTV} = \int_{\pi_f} \left|\nabla_f\right|_{Aw} dxdy \\ &= \int_{\pi_f} \sqrt{(A_x f_x)^2 + (A_y f_y)^2} dxdy \end{aligned} \tag{15}$$

where A_x and A_y are the adaptive weights of x-direction and y-direction. To reduce the computational complexity, we use the summation of the absolute of different difference values in different directions to simplify the AwTV model, and we can obtain the new representation of AwTV.

$$\begin{aligned}\Psi(f) &= \|f\|_{AwTV} = \int_{\pi_f} \left|\nabla_f\right|_{Aw} dxdy \\ &\approx \int_{\pi_f} |A_x f_x| + |A_y f_y| dxdy \end{aligned} \tag{16}$$

For the discrete model, the AwTv can be denoted as the following.

$$\begin{aligned}\Psi(f) &= \|f\|_{AwTV} = ||A_1 D_1 f||_1 + ||A_2 D_2 f||_1 \\ &= \sum_{i=1}^{2} ||A_i D_i f||_1 \end{aligned} \tag{17}$$

where i is the difference direction. A_i is a diagonal matrix and its diagonal elements denote the adaptive weights. D_i is the difference operator matrix.

For a 2-dimension image, each diagonal value in the adaptive matrix is defined as:

$$A_{1,i} = \omega(g_{i,j}, g_{i-1,j}) \tag{18}$$

$$A_{2,i} = \omega(g_{i,j}, g_{i,j1}) \tag{19}$$

where the weight function can be denoted as

$$\omega(a, b) = e^{\frac{-(a-b)^2}{\sigma^2}} \tag{20}$$

where σ is a parameter to control the smoothness of edge and the resolution of the reconstructed image. If σ is too large, the weights may tend to have the similar value, and the quality of reconstruction image based AwTV will be similar to the normal TV. If σ is too small, the weights may be very small in a direction, and the reconstruction image may generate some artifacts. Therefore, it is very important to select a proper value.

B. ADM-AWTV MODEL

According to AwTV and ADMTV, we combine AwTV and ADMM to construct the ADM-AwTV method. The objection function can be denoted as:

$$\begin{aligned} f^* &= \arg\min \|f\|_{AwTV} \\ &= \arg\min \sum_{i=1}^{2} ||A_i D_i f||_1 \\ &\text{s.t. } p = Wf \end{aligned} \tag{21}$$

where D_1 and D_2 denote two difference operator matrices on the horizontal and vertical directions. A_1 and A_2 are the adaptive weights on the horizontal and vertical directions.

Let $B_i = A_i D_i$, the objective function of (21) can be rewritten as the following.

$$\begin{aligned} f^* &= \arg\min \|f\|_{AwTV} \\ &= \arg\min \sum_{i=1}^{2} ||B_i f||_1 \\ &\text{s.t. } p = Wf \end{aligned} \tag{22}$$

where B_i is the adaptive weighted difference operator, which can reveal the anisotropy of reconstruction image.

C. OPTIMIZATION

For the optimization problem of the ADM-AwTV, we can use ADMM to obtain the optimized solution. Let $u_i = B_i f$, the problem of (22) can be denoted as

$$\begin{aligned} &\min \sum_{i=1}^{2} ||u_i||_1 \\ &\text{s.t. } p = Wf, u_i = B_i f \end{aligned} \tag{23}$$

With this sparse optimization problem, we can construct the Lagrangian function of (23) as:

$$\begin{aligned} &L(f, u_i, v_i, \lambda) \\ &= \sum_i \left(\|u_i\| - v_i^T (B_i f - u_i) + \frac{\beta_i}{2} \cdot \|B_i f - u_i\|_2^2 \right) \\ &\quad - \lambda^T (Wf - p) + \frac{\mu}{2} \cdot \|Wf - p\|_2^2 \end{aligned} \tag{24}$$

where β_i and μ are the parameters. v_i and λ are two Lagrangian multipliers vectors.

With the Lagrangian function, we can divide the sparse optimization problem of (24) into two subproblems, and they

can represented as

$$\min_{u_i} L(u_i) = \sum_i \left(\|u_i\|_1 - v_i^T (B_i f - u_i) + \frac{\beta_i}{2} \cdot \|B_i f - u_i\|_2^2 \right) \quad (25)$$

$$\min_f L(f) = \sum_i \left(-v_i^T (D_i f - u_i) + \frac{\beta_i}{2} \cdot \|D_i f - u_i\|_2^2 \right) - \lambda^T (Wf - p) + \frac{\mu}{2} \cdot \|Wf - p\|_2^2 \quad (26)$$

To obtain the optimized solution, we adopt the alternate iteration method to solve the subproblems. For the "u-subproblem", we use the iterative soft thresholding function to solve the l_1 optimization problem, which is a shrinkage operator shrinkage$(u, a) = \max\{|u| - a, 0\}\text{sign}(u)$, where sign$(u)$ is the sign function. Then, we can obtain the $(k+1)$-th iteration of (25).

$$u_i^{k+1} = \text{shrinkage}(B_i^k f^k - v_i^k/\beta_i, 1/\beta_i) = \max\left\{ \left| B_i^k f^k - \frac{v_i^k}{\beta_i} \right| - \frac{1}{\beta_i}, 0 \right\} \text{sign}(B_i^k f^k - \frac{v_i^k}{\beta_i}) \quad (27)$$

For the "f-subproblem", we set the partial derivative of f to zero, and the iteration function of (26) can be denoted as:

$$f^{k+1} = \left(\sum_i \beta_i (B_i^k)^T B_i^{k_i} + \mu W^T W \right)^+ \times \left(\sum_d \sum_i \left((B_i^k)^T v_i^k + \beta_i (B_i^k)^T u_i^{k+1} \right) + W^T \lambda^k + \mu W^T p \right) \quad (28)$$

For the Lagrangian multipliers vectors of (24), the updating in each iteration can be represented as:

$$v_i^{k+1} = v_i^k - \beta_i \left((B_i^k)^T f^{k+1} - u_i^{k+1} \right)$$
$$\lambda^{k+1} = \lambda^k - \mu \left(W f^{k+1} - p \right) \quad (29)$$

For the adaptive weighted difference operator of (22), the updating is defined as:

$$B_i^{k+1} = A_i^{k+1} D_i \quad (30)$$

The adaptive weights of (18) and (19) are denoted as the following updating.

$$A_{1,j}^{k+1} = \omega(g_{i,j}^{k+1}, g_{i-1,j}^{k+1}) \quad (31)$$
$$A_{2,j}^{k+1} = \omega(g_{i,j}^{k+1}, g_{i,j-1}^{k+1}) \quad (32)$$

where g^{k+1} is the 2- dimension form of f^{k+1}.

IV. EXPERIMENTS AND RESULTS

In this section, we will evaluate the performance of the ADM-AwTV algorithm under several limited angles. To demonstrate the effectiveness of our method, we will compare the proposed method with several other algorithms based on TV regularization including ART-TV and ADTVM, and the algorithms are conducted with the toolbox from http://web.eecs.umich.edu/~fessler/irt/irt/. At the same time, we will conduct some experiments on two simulation images and a real projection data. All the algorithms in the experiment were programmed using MATLAB language. The running software was MATLAB R2017b, and all experiments use the fan beam to obtain the projection matrix.

A. EVALUATION INDEX

In the simulation experiment, we use the Shepp-Logan phantom constructed by the computer as the original image (ground truth), and input the sinusoidal image generated by the phantom to each reconstruction algorithm. To evaluate the reconstruction effect of each algorithm, we calculate the root mean square error (RMSE), peak signal-to-noise ratio (PSNR), and structural similarity index (SSIM) between the reconstructed image and the original image [55]. The root mean square error is defined as follows:

$$RMSE = \sqrt{\frac{\sum_{i=1}^{N} \left(x_{i\_rec} - x_{i\_ori} \right)^2}{N}} \quad (33)$$

where N is the total number of pixels in the original image, x_{i_rec} and x_{i_ori} represent the i-th pixel values of the reconstructed image and the original image, respectively. The smaller the RMSE value is, the reconstructed image is closer to the original image, and the better the reconstruction result is.

The PSNR is defined as follows:

$$PSNR = 10 \log_{10} \left[\frac{(2^n - 1)^2}{RMSE^2} \right] \quad (34)$$

where n is the gray level of the image, it is 256 in general. The larger the PSNR value is, the reconstructed image is more similar to the original image.

The definition of SSIM is as follows:

$$SSIM = \frac{(2\mu_A \mu_B + c_1)(2\sigma_{AB} + c_2)}{(\mu_A^2 + \mu_B^2 + c_1)(\sigma_A^2 + \sigma_B^2 + c_2)} \quad (35)$$

where μ_A and μ_B are the average pixel values of the reconstruction image and the original image, respectively. σ_A and σ_B are the variances of the reconstruction image and the original image, respectively. σ_{AB} is the covariance between the reconstruction image and the original image. c_1 and c_2 are the constants used to stabilize the formula, and $c_1 = (k_1 L)^2$, $c_2 = (k_2 L)^2$, L is the dynamic range of pixel values, $k_1 = 0.01$, $k_2 = 0.03$. The value of SSIM is from 0 to 1. If the value is closer to 1, the reconstructed image has more similar structure to the original image.

B. SIMULATION EXPERIMENTS

The system parameters that need to be used in the simulation experiment are listed in Table 1.

TABLE 1. Simulation system parameters.

PARAMETER	VALUE
THE NUMBER OF DETECTOR UNITS	258
DETECTOR UNIT SIZE	1 mm
DISTANCE FROM X-RAY SOURCE TO DETECTORS	2061 mm
DISTANCE FROM X-RAY SOURCE TO CENTER OF ROTATION	1600 mm
SIZE OF RECONSTRUCTION IMAGE	128×128
PIXEL SIZE	1.56×1.56 mm^2

1) SIMULATION IMAGE 1

To compare the reconstruction quality of various algorithms, we can obtain the reconstruction image at three limited angles including 90°, 120° and 150°, and the results are shown in Figure 1.

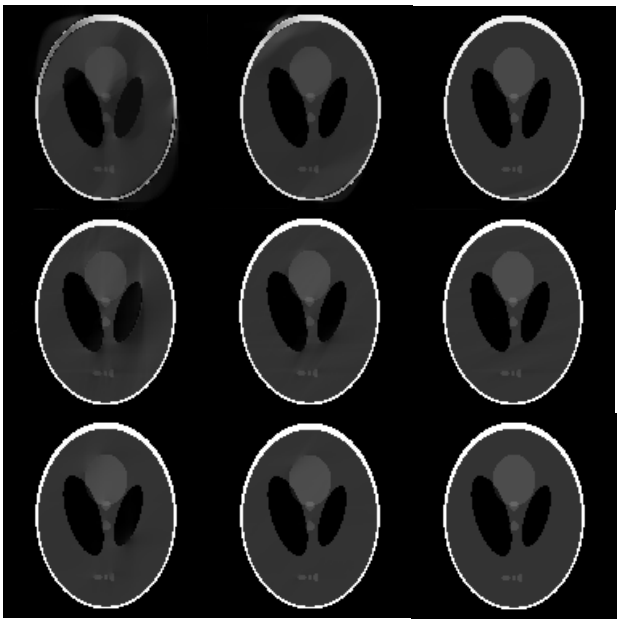

FIGURE 1. Reconstruction results of different algorithms for three limited angles with 100 iterations on the simulation image 1, where the first to third column are for the limited angles of 90°, 120°, and 150°, respectively; the first row is the reconstruction results of ART-TV, the second row is the reconstruction results of ADTVM, and the third row is the reconstruction results of ADM-AwTV.

According to Figure 1, the classic ART-TV algorithm has serious artifact in the reconstruction image at the limited angle of 90°. With the increasing of angle, the degree of artifact will gradually decrease, and the artifact is not completely eliminated even when the angle is increased to 150°. Compared with ART-TV, the reconstruction effect of ADTVM at limited angles has a certain improvement, but the reconstruction image still has artifacts at different limited angles. This artifacts also decrease when the scan angle increases. When the limited angle reaches 150°, the reconstruction image just has slight artifacts. Under the same limited angles, the proposed ADM-AwTV method shows the best reconstruction results than the other methods, because ADM-AwTV considers the anisotropy of image and constructs the adaptive weights on different directions.

To analyze the results of each algorithm, Table 2 shows the RMSE of each reconstruction image at different limited angles with 100 iterations.

TABLE 2. RMSE of different methods at different limited angles.

No.	Algorithm angles	90°	120°	150°
1	ART-TV	0.0664	0.0305	0.0061
2	ADTVM	0.0133	0.0054	0.0024
3	ADM-AwTV	**0.0059**	**0.0025**	**2.5587e-05**

TABLE 3. PSNR of different methods at different limited angles.

No.	Algorithm angles	90°	120°	150°
1	ART-TV	71.9566	78.4501	92.3778
2	ADTVM	127.7905	135.7058	142.5138
3	ADM-AwTV	134.9036	142.3212	182.1145

TABLE 4. SSIM of different methods at different limited angles.

No.	Algorithm angles	90°	120°	150°
1	ART-TV	0.8802	0.9684	0.9951
2	ADTVM	0.9616	0.9881	0.9969
3	ADM-AwTV	0.9875	0.9982	0.9999

According to Table 2, 3, and 4, the RMSE of ADM-AwTV is significantly smaller than ART-TV and ADTVM under the same limited angles, because AwTV can better reveal the anisotropy of image than the traditional TV. In addition, the PSNR and SSIM of ADM-AwTV are also superior to other two algorithms.

Figure 2 shows the RMSE of three algorithms with respect to the number of iterations at limited angles of 90°, 120°, and 150° with 100 iterations.

In Figure 2, it can be clearly seen from the partial enlarged detail that our method has faster convergence characteristics than the other algorithms. The RMSE decreases with the increasing of the number of iterations, and the ADM-AwTV has the smallest RMSE compared with ART-TV and ADMTV.

The center profile contrast experiment is usually used to compare the difference between the reconstructed image and the original image, and the center profile includes transverse center profile and longitudinal center profile. Figure 3 shows the center profiles of the reconstruction image in Figure 1. The results show the center profiles of the proposed method is the best similar to the original center profile at different limited angles.

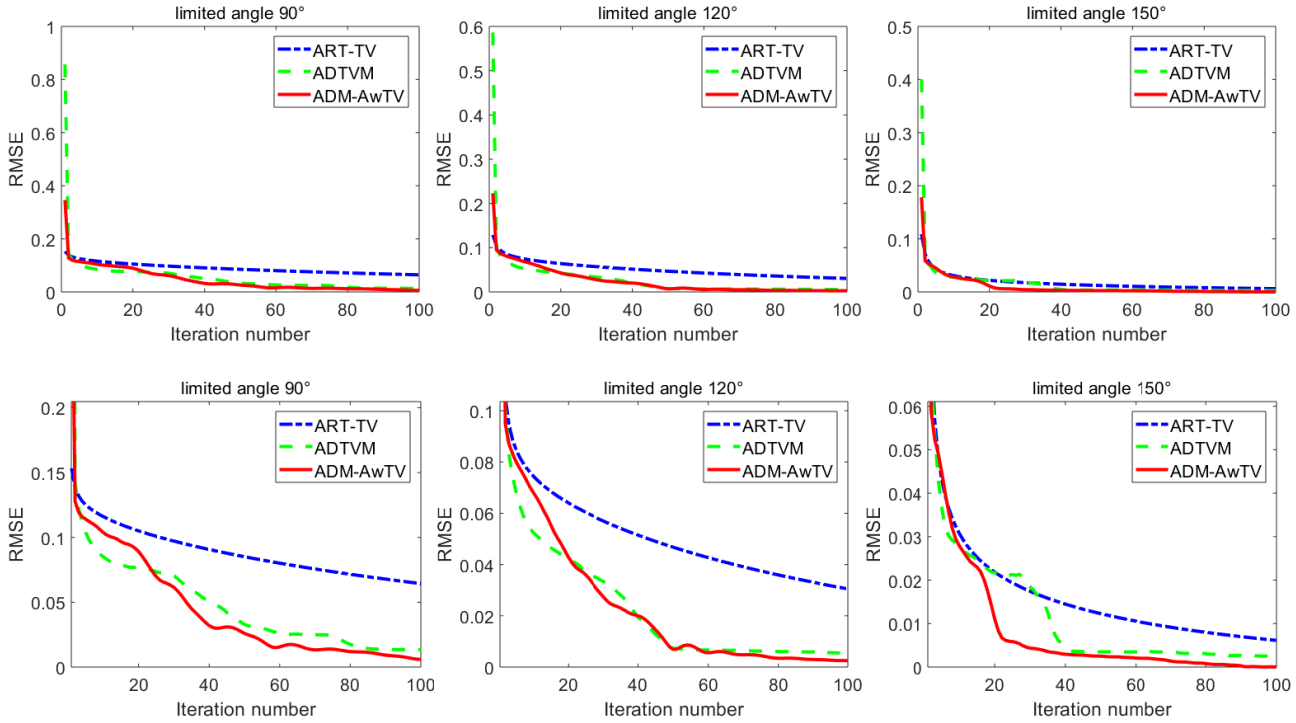

FIGURE 2. RMSE of ART-TV, ADTVM, and ADM-AwTV with respect to different numbers of iteration at different limited angles on the simulation image 1. From the first to third column, the limited angle is set to 90°, 120°, and 150°. The second row is the partial enlarged detail of the first row.

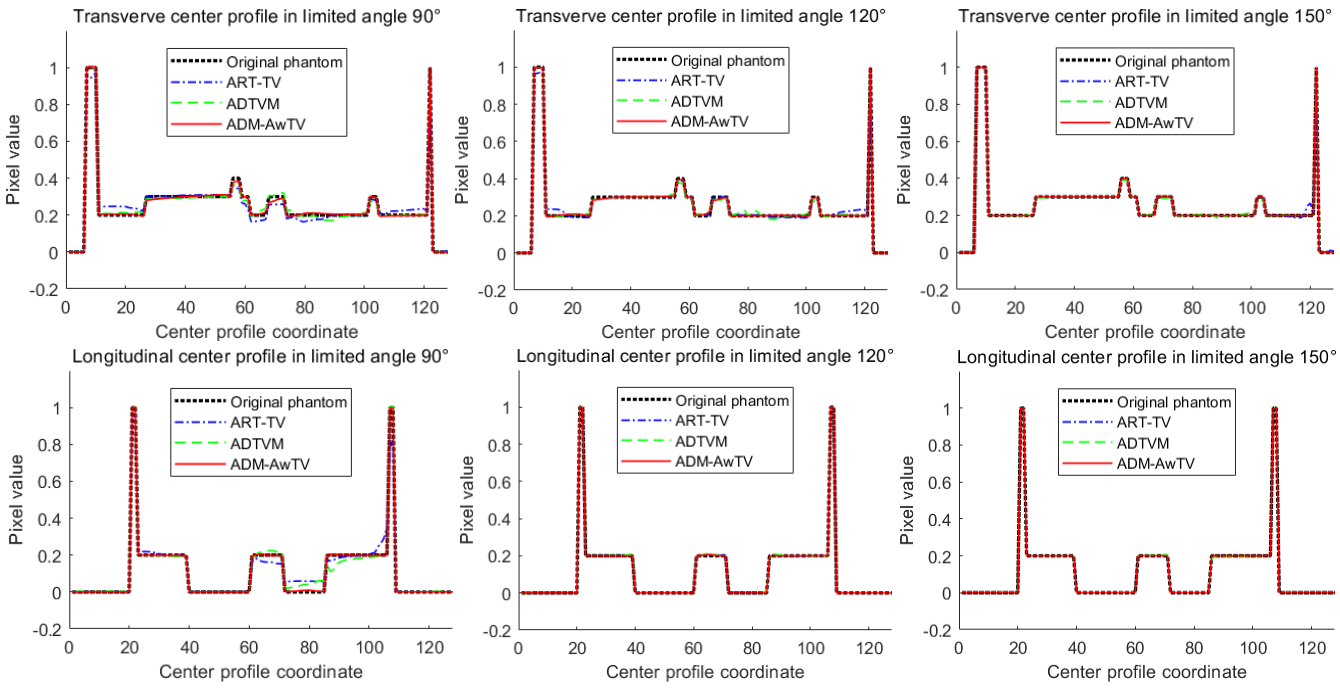

FIGURE 3. Center profiles of the reconstruction image with various algorithms at different limited angles on the simulation image 1. The first row is the transverse center profile comparison, and the second row is the longitudinal center profile comparison. From the first to third column, they are the reconstruction image at the limited angles of 90°, 120°, and 150°, respectively.

2) SIMULATION IMAGE 2

To further reveal the effectiveness of the proposed methods, we used another simulation image to conduct the experiment and termed it as simulation experiment 2. We also uses three limited angles, including 90°, 120°, and 150°, to perform the image reconstruction with different methods in Figure 4.

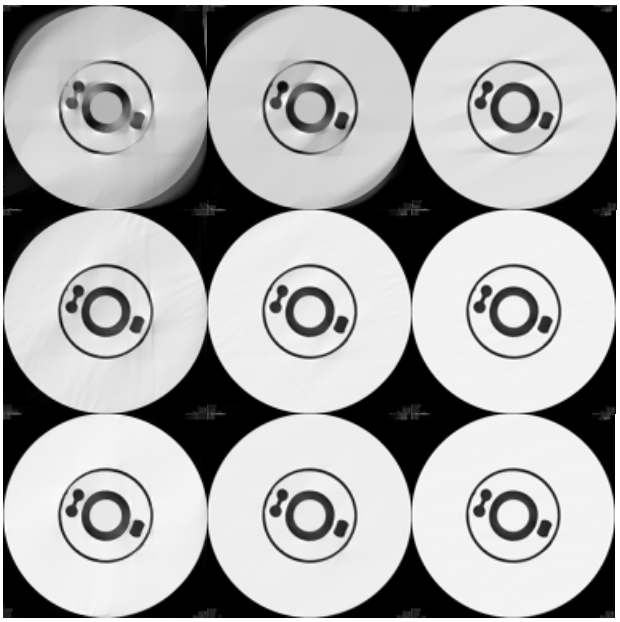

FIGURE 4. Reconstruction results of different algorithms for three limited angles with 100 iterations on the simulation image 2, where the first to third column are for the limited angles of 90°, 120°, and 150°, respectively; the first row is the reconstruction results of ART-TV, the second row is the reconstruction results of ADTVM, and the third row is the reconstruction results of ADM-AwTV.

From Figure 4, with the increasing of the scanning angle, the artifacts are gradually weakened. When the scanning angle is small, the reconstruction results of ART-TV have serious artifacts, and even the limited angle is 150°, there still exists a large number of artifacts in the reconstruction image. The ADMTV and ADM-AwTV methods generate better results than ART-TV in all conditions. Under the limited angle of 150°, ADM-AwTV and ADMTV obtains the similar reconstruction image. However, the reconstruction image of ADM-AwTV is superior to ADMTV and there is almost no artifacts for ADM-AwTV at the small scanning angle of 90°, which indicates that the proposed method has better performance of image reconstruction under a small scanning angle.

TABLE 5. RMSE of different algorithms under limited angles.

No.	Algorithm angles	90°	120°	150°
1	ART-TV	0.1285	0.0636	0.0250
2	ADTVM	0.0292	0.0130	0.0064
3	ADM-AwTV	0.0243	0.0117	0.0064

To analyze the quantitative results, Table 5, 6 and 7 display the RMSE, PSNR and SSIM of each image reconstructed algorithm at different limited angles with 100 iterations.

From Table 5, 6, and 7, we can draw the same conclusion as the simulation image 1. The reconstruction result of ADM-AwTV is better than that of ART-TV and ADTVM in most conditions.

TABLE 6. PSNR of different algorithms under limited angles.

No.	Algorithm angles	90°	120°	150°
1	ART-TV	65.9514	72.0677	80.1626
2	ADTVM	120.9820	127.9784	134.1890
3	ADM-AwTV	122.5603	128.8787	134.1321

TABLE 7. SSIM of different algorithms under limited angles.

No.	Algorithm angles	90°	120°	150°
1	ART-TV	0.7703	0.9194	0.9765
2	ADTVM	0.9307	0.9777	0.9886
3	ADM-AwTV	0.9636	0.9896	0.9932

Figure 5 shows the relationship of RMSE and the number of iterations. In the partial enlarged figure, ADM-AwTV and ADMTV have better RMSE than ART-TV, and the proposed ADM-AwTV method achieves the best results at the limited angles of 90°, 120°, and 150°.

To better show the difference between the reconstruction and the original image, the center profiles of Figure 4 are shown in Figure 6. The center profiles of ART-TV method exists a larger difference than that of the original image. The proposed method generates the best similar transverse and longitudinal center profiles to the ground truth image.

C. REAL PROJECTION DATA

For the difference of the projection data of the simulation image, the real projection data is obtained by scanning the real object with the CT system. The real projection data of this paper is from the scanning of a certain mechanical component with the industrial CT system. Therefore, the parameters of the CT system are different from the system parameters used in the previous simulation experiments, and the system parameters are listed in Table 8.

TABLE 8. System parameters for an industrial CT system.

PARAMETER	VALUE
THE NUMBER OF DETECTOR UNITS	1024
DETECTOR UNIT SIZE	0.227 mm
DISTANCE FROM X-RAY SOURCE TO DETECTORS	3578 mm
DISTANCE FROM X-RAY SOURCE TO CENTER OF ROTATION	568 mm
SIZE OF RECONSTRUCTION IMAGE	128×128
PIXEL SIZE	1.52×1.52 mm2

The projection datum of the limited angles are extracted from the completed sonogram that is obtained by selecting 1024 angles at equal intervals under the scanning angle of 360° for a real mechanical component with an industrial CT system, and the size of the projection data is 1024×1024. For the limited angle problem, we continuously select some angles from the 1024 angles according to the ratio of different

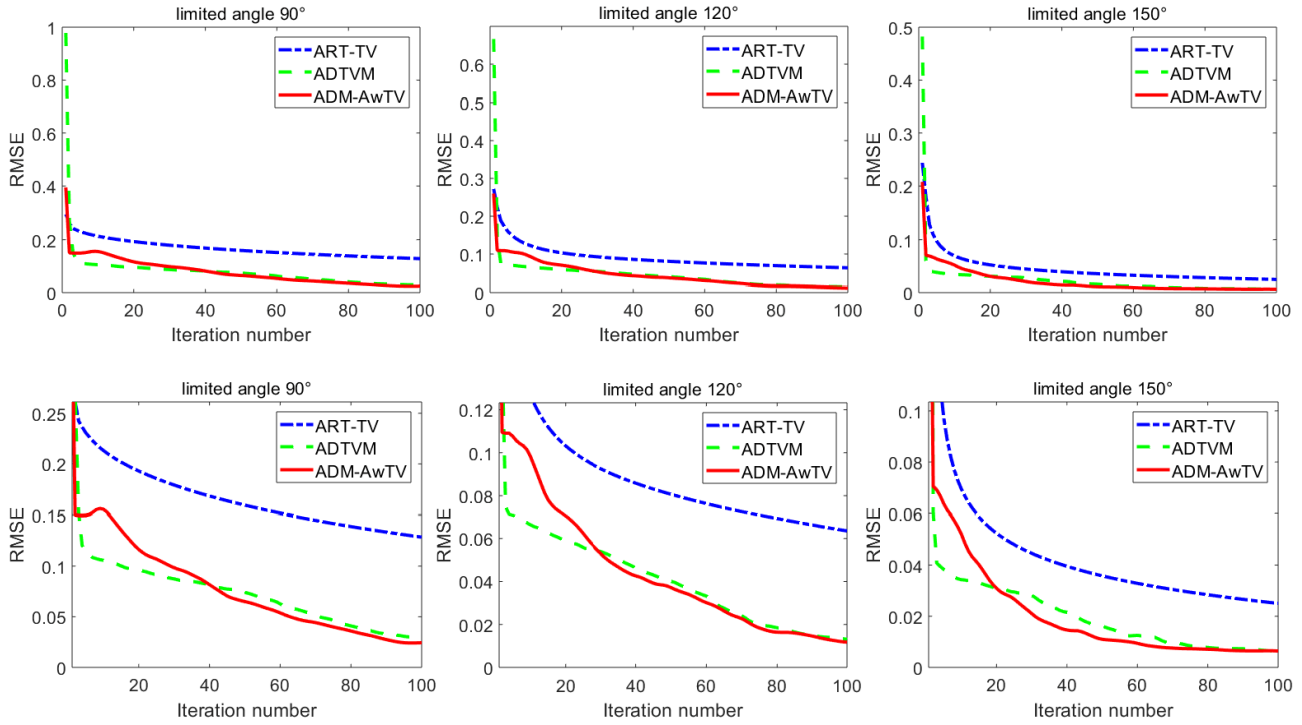

FIGURE 5. RMSE of ART-TV, ADTVM, and ADM-AwTV with respect to different numbers of iteration at different limited angles on the simulation image 2. From the first to third column, the limited angle is set to 90°, 120°, and 150°. The second row is the partial enlarged detail of the first row.

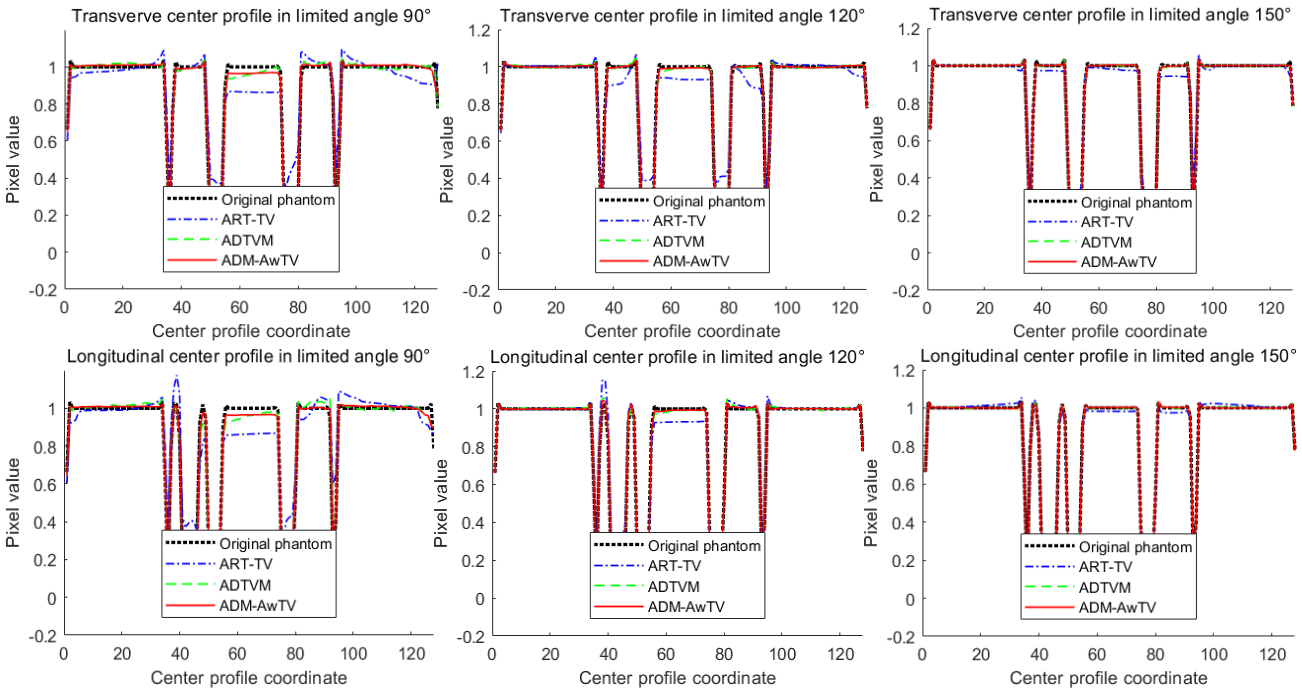

FIGURE 6. Center profiles of the reconstruction image with various algorithms at different limited angles on the simulation image 2. The first row is the transverse center profile comparison, and the second row is the longitudinal center profile comparison. From the first to third column, they are the reconstruction image at the limited angles of 90°, 120°, and 150°.

limited angles to 360°. Therefore, 90° is about 256 angles, 120° is approximate to 341 angles, and 150° is approximate to 427 angles.

In Figure 7, it shows the reconstruction results of the three algorithms with 100 iterations at different limited angles. From the reconstruction results, it can be seen that the

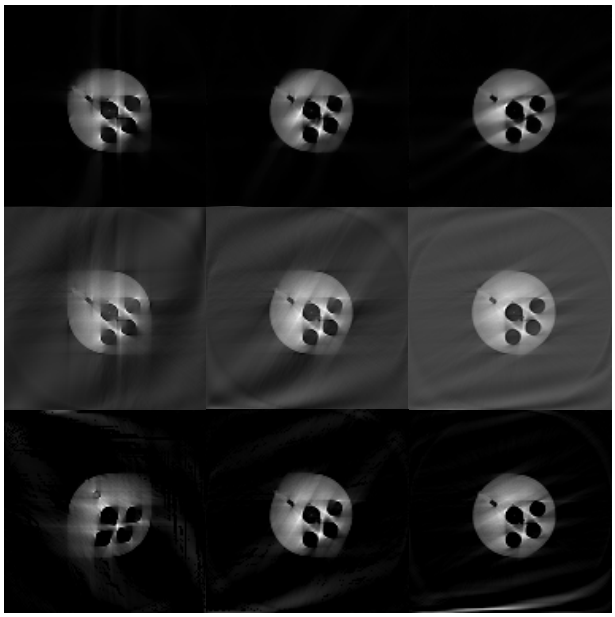

FIGURE 7. Reconstruction results of different algorithms for three limited angles with 100 iterations on the real projection data, where the first to third column are for the limited angles of 90°, 120°, and 150°, respectively; the first row is the reconstruction results of ART-TV, the second row is the reconstruction results of ADTVM, and the third row is the reconstruction results of ADM-AwTV.

reconstruction results of ADTVM and ADM-AwTV are better than that of ART-TV under the same limited angle. ART-TV has larger black artifacts at a limited angle, which seriously affects the quality of reconstructed images. The proposed ADM-AwTV method has better edges and weaker artifacts at the limited angles of 90° and 150°, especially in the outer edge regions of the mechanical component.

V. CONCLUSION

In this paper, we propose a CT image reconstruction algorithm based on ADMM and AwTV regularization and test the algorithm for the limited angle problem. Our algorithm is an improved algorithm of ADTVM, and we construct an adaptive weighted TV model which can adaptively reveal the anisotropic of image. In each iteration, the weights on different directions can update based on the last reconstruction image. The experiments on two simulation images and a real projection data demonstrate that the proposed algorithm has better reconstruction result than other algorithms for the limited angle problem. Although the proposed method achieves better results on the simulation image, it doesn't generate an obvious superiority for the real projection. Therefore, we will further improve the robustness of the TV model for the future.

REFERENCES

[1] W. Wu, H. Yu, C. Gong, and F. Liu, "Swinging multi-source industrial CT systems for aperiodic dynamic imaging," *Opt. Express*, vol. 25, no. 20, pp. 24215–24235, Oct. 2017.

[2] X. Qian *et al.*, "High resolution stationary digital breast tomosynthesis using distributed carbon nanotube X-ray source array," *Med. Phys.*, vol. 39, no. 4, pp. 2090–2099, Apr. 2012.

[3] P. E. Eppenberger, M. Cavka, M. E. Habicht, F. M. Galassi, and F. Rühli, "Radiological findings in ancient Egyptian canopic jars: comparing three standard clinical imaging modalities (X-rays, CT and MRI)," *Eur. Radiol.*, vol. 2, p. 12, Jun. 2018.

[4] J. Wang, Q. Qin, L. Guo, and Y. Feng, "Multi-fractal characteristics of three-dimensional distribution of reconstructed soil pores at opencast coal-mine dump based on high-precision CT scanning," *Soil Tillage Res.*, vol. 182, pp. 144–152, Oct. 2018.

[5] H. Scheffel *et al.*, "Accuracy of dual-source CT coronary angiography: first experience in a high pre-test probability population without heart rate control," *Eur. Radiol.*, vol. 16, no. 12, pp. 2739–2747, Sep. 2006.

[6] B. Du, M. Zhang, L. Zhang, R. Hu, and D. Tao, "PLTD: Patch-based low-rank tensor decomposition for hyperspectral images," *IEEE Trans. Multimedia*, vol. 19, no. 1, pp. 67–79, Jan. 2017.

[7] F. Luo, H. Huang, Y. Duan, J. Liu, and Y. Liao, "Local geometric structure feature for dimensionality reduction of hyperspectral imagery," *Remote Sens.*, vol. 9, no. 8, p. 790, Aug. 2017.

[8] B. Du, X. Tang, Z. Wang, L. Zhang, and D. Tao, "Robust graph-based semisupervised learning for noisy labeled data via maximum correntropy Criterion," *IEEE Trans. Cybern.*, to be published, doi: 10.1109/TCYB.2018.2804326.

[9] F. Luo, B. Du, L. Zhang, L. Zhang, and D. Tao, "Feature learning using spatial-spectral hypergraph discriminant analysis for hyperspectral image," *IEEE Trans. Cybern.*, to be published, doi: 10.1109/TCYB.2018.2810806.

[10] B. Du, W. Xiong, J. Wu, L. Zhang, L. Zhang, and D. Tao, "Stacked convolutional denoising auto-encoders for feature representation," *IEEE Trans. Cybern.*, vol. 47, no. 4, pp. 1017–1027, Apr. 2017.

[11] K. A. Abdullah, M. F. McEntee, W. Reed, and P. L. Kench, "Radiation dose and diagnostic image quality associated with iterative reconstruction in coronary CT angiography: A systematic review," *J. Med. Imag. Radiat. Oncol.*, vol. 60, no. 4, pp. 459–468, Aug. 2016.

[12] W. Wu, H. Yu, W. Cong, and F. Liu, "Theoretically exact backprojection filtration algorithm for multi-segment linear trajectory," *Phys. Med. Biol.*, vol. 63, no. 1, p. 015037, Jan. 2018.

[13] W. Wu, H. Yu, S. Wang, and F. Liu, "BPF-type region-of-interest reconstruction for parallel translational computed tomography," *J. X-Ray Sci. Technol.*, vol. 25, no. 3, pp. 487–504, Jan. 2017.

[14] A. Korn *et al.*, "Iterative reconstruction in head CT: Image quality of routine and low-dose protocols in comparison with standard filtered back-projection," *Amer. J. Neuroradiol.*, vol. 33, no. 2, pp. 218–224, Feb. 2012.

[15] F. E. Diehn *et al.*, "CT dental artifact: Comparison of an iterative metal artifact reduction technique with weighted filtered back-projection," *Acta Radiol.*, vol. 6, no. 11, pp. 1–8, Nov. 2017.

[16] P. K. Pandey, N. Naik, P. Munshi, and A. Pradhan, "Inherent error estimates for noisy-data discrimination and filter-specification in universal back-projection based photo-acoustic tomography," *Biomed. Phys. Eng. Express*, vol. 4, no. 3, p. 035002, Mar. 2018.

[17] J. F. Barrett and N. Keat, "Artifacts in CT: Recognition and avoidance," *Radiographics*, vol. 24, no. 6, pp. 1679–1691, Dec. 2004.

[18] C. Kim *et al.*, "The optimal energy level of virtual monochromatic images from spectral CT for reducing beam-hardening artifacts due to contrast media in the thorax," *Amer. J. Neuroradiol.*, vol. 211, no. 3, pp. 557–563, 2018, doi: 10.2214/AJR.17.19377.

[19] A. H. Andersen, "Algebraic reconstruction in CT from limited views," *IEEE Trans. Med. Imag.*, vol. 8, no. 1, pp. 50–55, Mar. 1989.

[20] G. T. Herman and L. B. Meyer, "Algebraic reconstruction techniques can be made computationally efficient (positron emission tomography application)," *IEEE Trans. Med. Imag.*, vol. 12, no. 3, pp. 600–609, Sep. 1993.

[21] B. Liu *et al.*, "Image reconstruction from limited angle projections collected by multisource interior X-ray imaging systems," *Phys. Med. Biol.*, vol. 56, no. 19, pp. 6337–6357, Oct. 2011.

[22] Y. Zhao, X. Zhao, and P. Zhang, "An extended algebraic reconstruction technique (E-ART) for dual spectral CT," *IEEE Trans. Med. Imag.*, vol. 34, no. 3, pp. 761–768, Mar. 2015.

[23] B. Du, Z. Wang, L. Zhang, L. Zhang, and D. Tao, "Robust and discriminative labeling for multi-label active learning based on maximum correntropy criterion," *IEEE Trans. Image Process.*, vol. 26, no. 4, pp. 1694–1707, Apr. 2017.

[24] S. R. Tornga, M. W. R. Sullivan, and J. P. Sullivan, "Three-dimensional compton imaging using list-mode maximum likelihood expectation maximization," *IEEE Trans. Nucl. Sci.*, vol. 56, no. 3, pp. 1372–1376, Jun. 2009.

[25] B. Du and Y. Zhang, "Beyond the sparsity-based target detector: A hybrid sparsity and statistics based detector for hyperspectral images," *IEEE Trans. Image Process.*, vol. 25, no. 11, pp. 5345–5357, Nov. 2016.
[26] W. Wu, Y. Zhang, Q. Wang, F. Liu, F. Luo, and H. Yu, "Spatial-spectral cube matching frame for spectral CT reconstruction," *Inverse Problems*, vol. 34, no. 10, p. 104003, Jul. 2018.
[27] S. Niu, G. Yu, J. Ma, and J. Wang, "Nonlocal low-rank and sparse matrix decomposition for spectral CT reconstruction," *Inverse Problems*, vol. 34, no. 2, p. 024003, Feb. 2018.
[28] C. Jiang, Q. Zhang, R. Fan, and Z. Hu, "Super-resolution CT image reconstruction based on dictionary learning and sparse representation," *Sci. Rep.*, vol. 8, p. 8799, Jun. 2018.
[29] K. Choi, R. Li, H. Nam, and L. Xing, "A Fourier-based compressed sensing technique for accelerated CT image reconstruction using first-order methods," *Phys. Med. Biol.*, vol. 59, no. 12, pp. 3097–3119, Jun. 2014.
[30] T. Niu, X. Ye, Q. Fruhauf, M. Petrongolo, and L. Zhu, "Accelerated barrier optimization compressed sensing (ABOCS) for CT reconstruction with improved convergence," *Phys. Med. Biol.*, vol. 59, no. 7, pp. 1801–1814, Apr. 2014.
[31] J. Wen, Z. Zhou, J. Wang, X. Tang, and Q. Mo, "A sharp condition for exact support recovery with orthogonal matching pursuit," *IEEE Trans. Signal Process.*, vol. 65, no. 6, pp. 1370–1382, Mar. 2017.
[32] J. Wen, J. Wang, and Q. Zhang, "Nearly optimal bounds for orthogonal least squares," *IEEE Trans. Signal Process.*, vol. 65, no. 20, pp. 5347–5356, Oct. 2017.
[33] J. Wen, D. Li, and F. Zhu, "Stable recovery of sparse signals via ℓ_p-minimization," *Appl. Comput. Harmon. Anal.*, vol. 38, no. 1, pp. 161–176, Jan. 2015.
[34] G.-H. Chen, J. Tang, and S. Leng, "Prior image constrained compressed sensing (PICCS): A method to accurately reconstruct dynamic CT images from highly undersampled projection data sets," *Med. Phys.*, vol. 35, no. 2, pp. 660–663, 2008.
[35] P. Bannas *et al.*, "Prior image constrained compressed sensing metal artifact reduction (piccs-mar): 2D and 3D image quality improvement with hip prostheses at CT colonography," *Eur. Radiol.*, vol. 26, no. 7, pp. 2039–2046, Jul. 2016.
[36] Z. Yu, S. Leng, Z. Li, and C. H. McCollough, "Spectral prior image constrained compressed sensing (spectral PICCS) for photon-counting computed tomography," *Phys. Med. Biol.*, vol. 61, no. 18, pp. 6707–6732, Sep. 2016.
[37] J. Peng, D. Zeng, J. Ma, Y. Wang, and D. Meng, "CPCT-LRTDTV: Cerebral perfusion CT image restoration via a low rank tensor decomposition with total variation regularization," *Proc. SPIE*, vol. 10573, p. 1057337, Mar. 2018.
[38] S. Seyyedi *et al.*, "Component-based TV regularization for X-ray tensor tomography," in *Proc. IEEE 13th Int. Symp. Biomed. Imag. (ISBI)*, Apr. 2016, pp. 581–584.
[39] Z. Zhou *et al.*, "Comparison of total variation algorithms for electrical impedance tomography," *Physiol. Meas.*, vol. 36, no. 6, p. 1193, May 2015.
[40] B. Du *et al.*, "Exploring representativeness and informativeness for active learning," *IEEE Trans. Cybern.*, vol. 47, no. 1, pp. 14–26, Jan. 2017.
[41] H. Kim, J. Chen, A. Wang, C. Chuang, M. Held, and J. Pouliot, "Non-local total-variation (NLTV) minimization combined with reweighted L1-norm for compressed sensing CT reconstruction," *Phys. Med. Biol.*, vol. 61, no. 18, pp. 6878–6891, Sep. 2016.
[42] S. Tong *et al.*, "RTE-based parameter reconstruction with TV plus L1 regularization," *J. Comput. Appl. Math.*, vol. 337, pp. 256–273, Aug. 2018.
[43] A. Cai, Y. Hu, Z. Zheng, L. Li, and B. Yan, "Block-matching local SVD operator-based sparsity and TV regularization for image reconstruction in computed tomography," *Sens. Imag.*, vol. 19, p. 18, Dec. 2018.
[44] F. Mahmood, N. Shahid, U. Skoglund, and P. Vandergheynst, "Adaptive graph-based total variation for tomographic reconstructions," *IEEE Signal Process. Lett.*, vol. 25, no. 5, pp. 700–704, May 2018.
[45] N. Shahid, N. Shahid, P. Vandergheynst, and U. Skoglund, "Graph-based sinogram denoising for tomographic reconstructions," in *Proc. EMBC*, Aug. 2016, pp. 3664–3961.
[46] T. Wang, K. Nakamoto, H. Zhang, and H. Liu, "Reweighted anisotropic total variation minimization for limited-angle CT reconstruction," *IEEE Trans. Nucl. Sci.*, vol. 64, no. 10, pp. 2742–2760, Oct. 2017.
[47] S. Chen, H. Liu, Z. Hu, H. Zhang, P. Shi, and Y. Chen, "Simultaneous reconstruction and segmentation of dynamic PET via low-rank and sparse matrix decomposition," *IEEE Trans. Biomed. Eng.*, vol. 62, no. 7, pp. 1784–1795, Jul. 2015.
[48] B. Du and L. Zhang, "A discriminative metric learning based anomaly detection method," *IEEE Trans. Geosci. Remote Sens.*, vol. 52, no. 11, pp. 6844–6857, Nov. 2014.
[49] W. Lin-Yuan, Z. Han-Ming, C. Ai-Long, Y. Bin, L. Lei, and H. Guo-En, "Image reconstruction algorithm based on inexact alternating direction total-variation minimization," *Acta Phys. Sin.*, vol. 62, no. 19, p. 198701, Jun. 2013.
[50] Y. Wang, J. Yang, W. Yin, and Y. Zhang, "A new alternating minimization algorithm for total variation image reconstruction," *SIAM J. Imag. Sci.*, vol. 1, no. 3, pp. 248–272, Jul. 2008.
[51] Z. Wu, M. Li, D. Z. W. Wang, and D. Han, "A symmetric alternating direction method of multipliers for separable nonconvex minimization problems," *Asia–Pacific J. Oper. Res.*, vol. 34, no. 6, p. 1750030, 2017.
[52] X. Chen, Y. Di, J. Duan, and D. Li, "Linearized compact ADI schemes for nonlinear time-fractional Schrödinger equations," *Appl. Math. Lett.*, vol. 84, pp. 160–167, Oct. 2018.
[53] F. Wu, X. Cheng, D. Li, and J. Duan, "A two-level linearized compact ADI scheme for two-dimensional nonlinear reaction–diffusion equations," *Comput. Math. Appl.*, vol. 75, no. 8, pp. 2835–2850, Apr. 2018.
[54] M. Wang, D. Li, C. Zhang, and Y. Tang, "Long time behavior of solutions of gKdV equations," *J. Math. Anal. Appl.*, vol. 390, no. 1, pp. 136–150, Jun. 2012.
[55] L. Ritschl, F. Bergner, C. Fleischmann, and M. Kachelrieß, "Improved total variation-based CT image reconstruction applied to clinical data," *Phys. Med. Biol.*, vol. 56, no. 6, pp. 1545–1561, Jan. 2011.
[56] E. Y. Sidky and X. Pan, "Image reconstruction in circular cone-beam computed tomography by constrained, total-variation minimization," *Phys. Med. Biol.*, vol. 53, no. 17, pp. 4777–4807, Aug. 2008.
[57] Z. Chen, X. Jin, L. Li, and G. Wang, "A limited-angle CT reconstruction method based on anisotropic TV minimization," *Phys. Med. Biol.*, vol. 58, no. 7, pp. 2119–2141, Apr. 2013.
[58] Y. Liu, J. Ma, Y. Fan, and Z. Liang, "Adaptive-weighted total variation minimization for sparse data toward low-dose X-ray computed tomography image reconstruction," *Phys. Med. Biol.*, vol. 57, no. 23, pp. 7923–7956, Dec. 2012.
[59] W. Wu, Y. Zhang, Q. Wang, F. Liu, P. Chen, and H. Yu, "Low-dose spectral CT reconstruction using image gradient ℓ_0–norm and tensor dictionary," *Appl. Math. Model.*, vol. 63, pp. 538–557, Nov. 2018.
[60] D. Donoho, "Compressed sensing," *IEEE Trans. Inf. Theory*, vol. 52, no. 4, pp. 1289–1306, Apr. 2006.
[61] S. Boyd *et al.*, "Distributed optimization and statistical learning via the alternating direction method of multipliers," *Found. Trends Mach. Learn.*, vol. 3, no. 1, pp. 1–122, 2006.

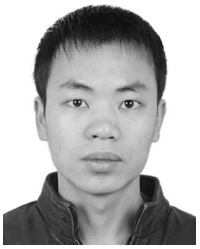

FULIN LUO (S'16–M'18) received the M.S. and Ph.D. degrees in instrument science and technology from Chongqing University, Chongqing, China, in 2013 and 2016, respectively.

He is currently a Post-Doctoral Researcher with the State Key Laboratory of Information Engineering in Surveying, Mapping and Remote Sensing, Wuhan University. His research interests are image processing and sparse representation.

WEICHEN LI received the B.S. degree in information safety from Hubei University, Wuhan, China, in 2017.

He is currently pursuing the master's degree with the School of Computer Science, Wuhan University. His research interests are computed tomography image reconstruction.

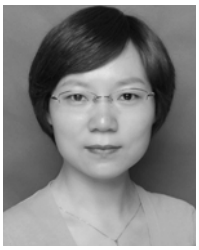

WEIPING TU received the M.S. and Ph.D. degrees in communication and information system from Wuhan University, Wuhan, China, in 2002 and 2011, respectively.

She is currently an Associate Professor with the National Engineering Research Center for Multimedia Software, Wuhan University. Her research interests are audio signal classification, speech separation, and image processing.

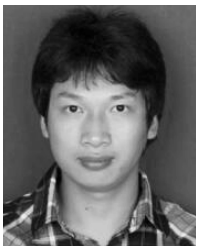

WEIWEN WU received the B.S. degree in measurement-control technology and instrumentation from Nanchang Hangkong University, Nanchang, China, in 2014. He is currently pursuing the Ph.D. degree with Chongqing University. His research interests are computed tomography (CT) image reconstruction, spectral CT reconstruction, dynamic bowties, and CT system design.